Stem Cell Reports
Article

ISSCR

OPEN ACCESS

# Pluripotent Stem Cell-Derived Cerebral Organoids Reveal Human Oligodendrogenesis with Dorsal and Ventral Origins

Hyosung Kim,[1] Ranjie Xu,[1] Ragunathan Padmashri,[2] Anna Dunaevsky,[2] Ying Liu,[3] Cheryl F. Dreyfus,[4] and Peng Jiang[1,*]

[1]Department of Cell Biology and Neuroscience, Rutgers University, Piscataway, NJ 08854, USA
[2]Department of Neurological Sciences, University of Nebraska Medical Center, Omaha, NE 68198, USA
[3]Department of Neurosurgery and Center for Stem Cell and Regenerative Medicine, the Brown Foundation Institute of Molecular Medicine for the Prevention of Human Diseases, University of Texas Health Science Center at Houston, Houston, TX 77030, USA
[4]Department of Neuroscience and Cell Biology, Rutgers Robert Wood Johnson Medical School, Piscataway, NJ 08854, USA
*Correspondence: peng.jiang@rutgers.edu
https://doi.org/10.1016/j.stemcr.2019.04.011

## SUMMARY

The process of oligodendrogenesis has been relatively well delineated in the rodent brain. However, it remains unknown whether analogous developmental processes are manifested in the human brain. Here we report oligodendrogenesis in forebrain organoids, generated by using OLIG2-GFP knockin human pluripotent stem cell (hPSC) reporter lines. OLIG2/GFP exhibits distinct temporal expression patterns in ventral forebrain organoids (VFOs) versus dorsal forebrain organoids (DFOs). Interestingly, oligodendrogenesis can be induced in both VFOs and DFOs after neuronal maturation. Assembling VFOs and DFOs to generate fused forebrain organoids (FFOs) promotes oligodendroglia maturation. Furthermore, dorsally derived oligodendroglial cells outcompete ventrally derived oligodendroglia and become dominant in FFOs after long-term culture. Thus, our organoid models reveal human oligodendrogenesis with ventral and dorsal origins. These models will serve to study the phenotypic and functional differences between human ventrally and dorsally derived oligodendroglia and to reveal mechanisms of diseases associated with cortical myelin defects.

## INTRODUCTION

Oligodendrocytes (OLs) are the myelinating cells and are the last major type of neural cells formed during CNS development (Goldman and Kuypers, 2015; Zhong et al., 2018). Much of our current knowledge on OL development is obtained from studies in rodents. There are three distinct and sequential waves of oligodendrogenesis. Starting at embryonic day 12.5 (E12.5), the first wave arises from NKX2.1-expressing precursors in the medial ganglionic eminence (Tekki-Kessaris et al., 2001). These oligodendrocyte progenitor cells (OPCs) migrate tangentially to distant locations and colonize the entire forebrain (Kessaris et al., 2006; Klambt, 2009). Subsequently, at E15.5 a second wave emerges from precursors in the lateral and medial ganglionic eminences (Chapman et al., 2013). These OPCs also migrate to the cortex, dispersing throughout the forebrain (Kessaris et al., 2006; Klambt, 2009). These ventrally derived OPCs either remain as OPCs or differentiate into myelinating OLs in the maturing neocortex (Kessaris et al., 2006; Tripathi et al., 2011). Around birth, a third wave arises dorsally from precursors expressing the homeobox gene EMX1 in the cortex (Kessaris et al., 2006; Winkler et al., 2018). Interestingly, these dorsally derived OPCs migrate locally to populate the cortex and displace the OPCs from the first two waves that initially colonize the cortical mantle (Kessaris et al., 2006; Winkler et al., 2018). Although the process of oligodendrogenesis has been well delineated in the mouse brain, it remains unknown whether analogous developmental processes are manifested in the human brain, particularly the dorsally derived third wave of oligodendrogenesis (Jakovcevski et al., 2009; Rakic and Zecevic, 2003).

The lack of human brain tissue prevents a detailed understanding of human oligodendrogenesis. Neural specification of human pluripotent stem cells (hPSCs), including human embryonic stem cells (hESCs) and human induced pluripotent stem cells (hiPSCs), offers unprecedented opportunities for studying human neural development (Avior et al., 2016; Marchetto et al., 2011). While OPCs have been efficiently derived from hPSC in the two-dimensional (2D) culture system, these OPCs are mainly derived from ventral CNS regions by using ventralizing morphogens, such as sonic hedgehog (SHH) (Goldman and Kuypers, 2015; Tao and Zhang, 2016). Despite previous progress, the different origins of human oligodendrogenesis have not been able to be recapitulated in 2D cultures, likely due to the lack of cell-cell/cell-matrix interactions in these monolayer cultures.

The recent development of 3D cerebral organoids derived from hPSCs offers a promising approach to understanding human brain development (Pasca, 2018), complementing 2D cell-culture models. In this study, using OLIG2-GFP knockin hPSC reporter lines (Liu et al., 2011), we generated brain region-specific dorsal forebrain organoids (DFOs) and ventral forebrain organoids (VFOs) by inhibiting or activating SHH signaling pathway, respectively. We further monitored the temporal expression of OLIG2 and examined the oligodendrogenesis in these brain

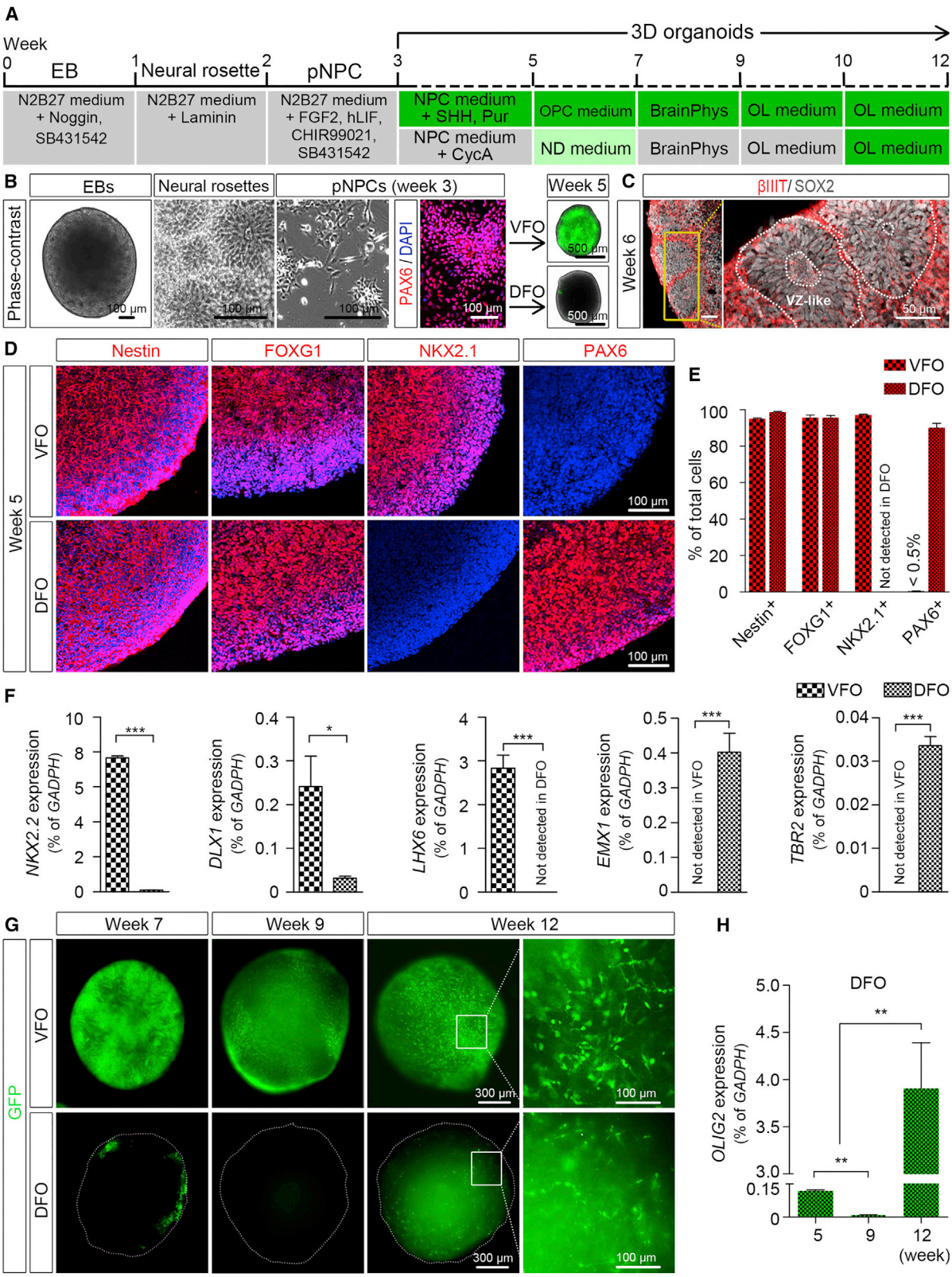


*(legend on next page)*

region-specific organoids. Moreover, by assembling DFOs and VFOs to form fused forebrain organoids (FFOs), we found that the human oligodendroglial differentiation and maturation were significantly promoted.

## RESULTS

### Distinct Expression Patterns of OLIG2 in hPSC-Derived Ventral and Dorsal Forebrain Organoids

To examine the expression of OLIG2 in brain region-specific organoids, we generated human VFOs and DFOs using OLIG2-GFP hPSC (hESC and hiPSC) reporter lines generated in our previous studies (Figures 1A and 1B) (Liu et al., 2011; Xue et al., 2009). Using methods established in recent studies (Bagley et al., 2017; Birey et al., 2017; Xiang et al., 2017), brain region-specific organoids were derived by either activating or inhibiting the SHH signaling pathway from week 3 to week 5. After one additional week of culturing with neural differentiation (ND) medium or OPC medium (week 6), both DFOs and VFOs exhibited subventricular/ventricular zone-like regions containing $SOX2^+$ neural progenitor cells (NPCs) and $\beta IIIT^+$ immature neurons (Figure 1C). As shown in Figures 1D and 1E, at week 5 both VFOs and DFOs were composed of a comparable population of Nestin-positive NPCs and FOXG1-positive forebrain cells. The vast majority of the cells in DFOs remained to express PAX6, which is also a marker for the NPCs in dorsal brain, whereas the vast majority of the cells in VFOs expressed NKX2.1, a marker of ventral prosencephalic progenitors. We further examined the gene expression of markers for dorsal forebrain, including *EMX1* and *TBR2*, and markers for ventral forebrain, including *NKX2.2*, *DLX1*, and *LHX6* in both DFOs and VFOs. EMX1 and TBR2 are expressed by cortical NPCs and intermediate progenitors (Englund et al., 2005; Gorski et al., 2002). NKX2.2, LHX6, and DLX1 are expressed by the NPCs in the medial ganglionic eminence (Briscoe et al., 1999; Du et al., 2008; Petryniak et al., 2007). As shown in Figure 1F, markers for ventral forebrain, *NKX2.2*, *DLX1*, and *LHX6*, were conspicuously detected in VFOs, whereas markers for dorsal forebrain, *EMX1* and *TBR2*, were restricted to DFOs. Although DFOs and VFOs were generated from the same population of $PAX6^+$ primitive NPCs (pNPCs) at week 3 (Figure 1B), as opposed to week-5 DFOs, nearly all the cells in week-5 VFOs were $NKX2.1^+/PAX6^-$ and abundantly expressed *NKX2.2*, *DLX1*, and *LHX6*, indicating that VFOs undergo ventral forebrain development induced by the activation of the SHH signaling pathway. Together with the data showing the restricted expression of *EMX1* and *TBR2* in DFOs, the observation that week-5 DFOs were highly enriched with $PAX6^+/NKX2.1^-$ NPCs indicates the formation of dorsal forebrain regional identity in DFOs. From week 5 to week 7, intense GFP signals were observed in VFOs, whereas a small subset of cells in DFOs was found to express GFP (Figures 1B and 1G). After long-term culture, robust GFP fluorescence in the VFOs became dimmer at week 9 and eventually was found to distribute evenly in the VFOs at week 12. The weak GFP signals in the DFOs gradually decreased and became undetectable at week 9. Interestingly, we observed the reappearance of GFP signals at week 12 (Figure 1G). Furthermore, we confirmed the *OLIG2* expression in DFOs by qRT-PCR. We consistently found that *OLIG2* expression was very low at week 5 and hardly detectable at week 9. At week 12, the *OLIG2* expression significantly increased about 25-fold compared with its level at week 5 (Figure 1H).

### OLIG2 Is Cytoplasmically Expressed in $PAX6^+$ Neural Progenitors in Week-5 DFOs

GFP signals faithfully mirrored the OLIG2 expression in organoids (Figures 2A and 2B). There was a significantly

**Figure 1. Temporal Expression of OLIG2 in hPSC-Derived VFOs and DFOs**

(A) A schematic procedure for deriving brain region-specific forebrain organoids from OLIG2-GFP hPSCs by the treatment of a combination of sonic hedgehog (SHH) and purmorphamine (Pur) or cyclopamine (CycA) alone for VFOs and DFOs, respectively. The stages after week 3 are color coded based on the expression of GFP.

(B) Representative bright-field and fluorescence images of embryoid bodies (EBs) at week 1, neural rosettes at week 2, primitive neural progenitor cells (pNPCs) at week 3, and VFOs and DFOs at week 5. pNPCs at week 3 were positive for PAX6 staining. Scale bars, 100 μm for bright-field images and 500 μm for fluorescence images.

(C) Representatives of the ventricular zone (VZ)-like structure formed by $\beta IIIT^+$ and $SOX2^+$ cells in DFOs at week 6. Scale bars, 50 μm.

(D and E) Representatives (D) and quantification (E) of Nestin-, FOXG1-, NKX2.1-, and PAX6-expressing cells in week-5 VFOs or DFOs (n = 4 organoids from two hPSC lines).

(F) qRT-PCR results showing the expression of *NKX2.2*, *DLX1*, *LHX6*, *EMX1*, and *TBR2* in week-5 VFOs and DFOs (n = 3 independent experiments). Student's t test: $^{**}p < 0.05$ and $^{***}p < 0.001$.

(G) Temporal expression of GFP fluorescence in VFOs and DFOs. Scale bars, 300 μm in the original images and 100 μm in the enlarged images.

(H) qRT-PCR results showing the expression of *OLIG2* at different time points in the DFOs. The expression level is normalized to GAPDH (n = 4 independent experiments). One-way ANOVA with Turkey's post hoc test: $^{**}p < 0.01$.

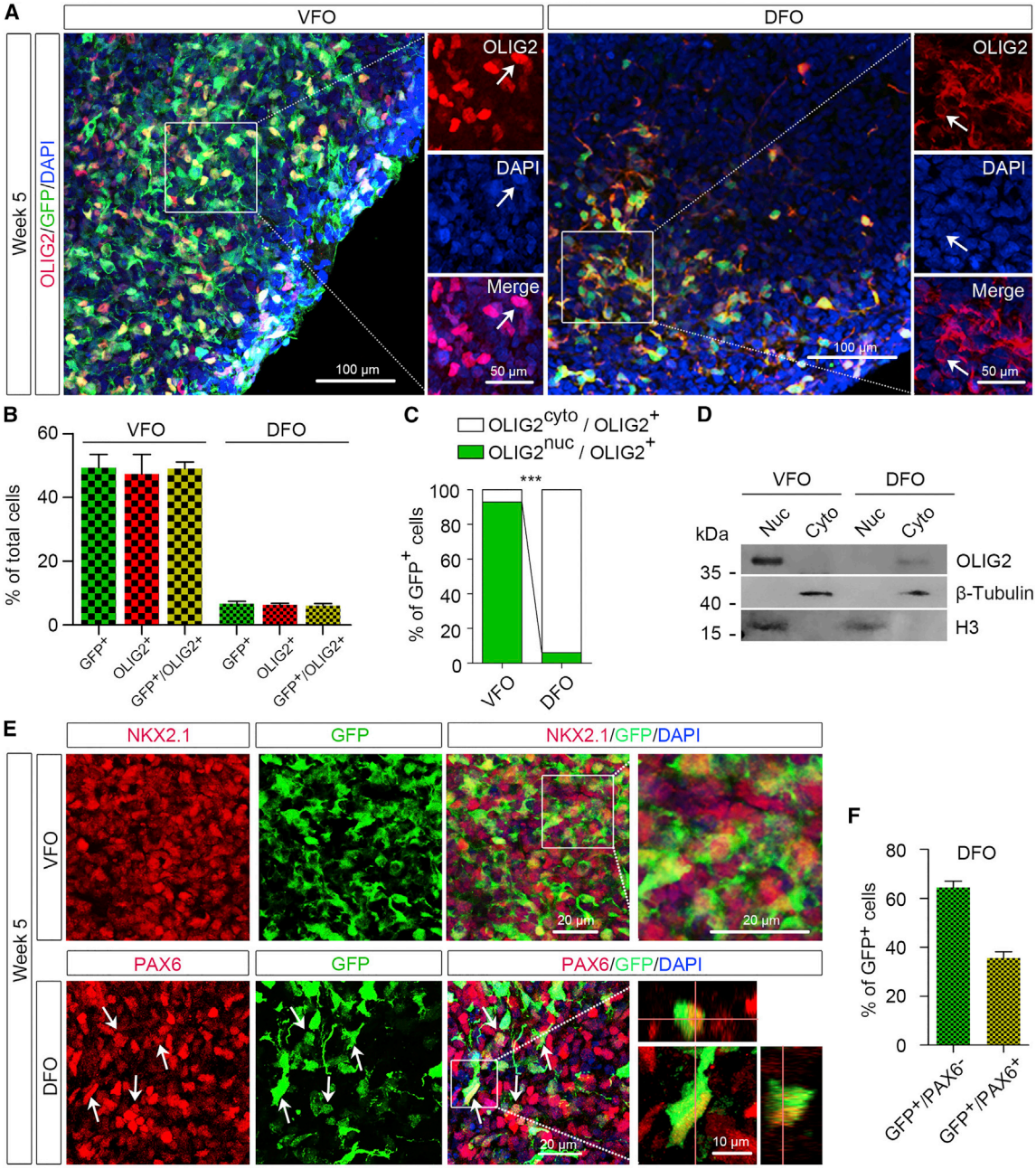


**Figure 2. Cellular Localization of OLIG2 in VFOs and DFOs**

(A and B) Representatives (A) and quantification (B) of GFP$^+$, OLIG2$^+$, and GFP$^+$/OLIG2$^+$ cells in the VFOs and DFOs at week 5 (n = 4 organoids from two hPSC lines). Scale bars, 100 μm in the original images and 50 μm in the enlarged images.

(C) Quantification of the percentage of GFP$^+$ cells with nuclear or cytoplasmic OLIG2 expression among total GFP$^+$ cells (n = 3 organoids from two hPSC lines). Student's t test: ***p < 0.001.

(D) Western blot showing the cellular localization of OLIG2 extracted from week-5 organoids. The experiments were repeated three times. For each experiment, at least ten VFOs or DFOs derived from OLIG2-GFP hESCs and hiPSCs were pooled for protein extraction and fractionation.

(E) Representative images of NKX2.1$^+$/GFP$^+$ cells in VFOs (top panels) and PAX6$^+$/GFP$^+$ cells in DFO (bottom panels). Scale bars, 50 μm in the original images and 10 μm in the enlarged images.

(F) Quantification of percentage of GFP$^+$/PAX6$^-$ cells and GFP$^+$/PAX6$^+$ cells in week-5 DFOs (n = 5 organoids from two hPSC lines).

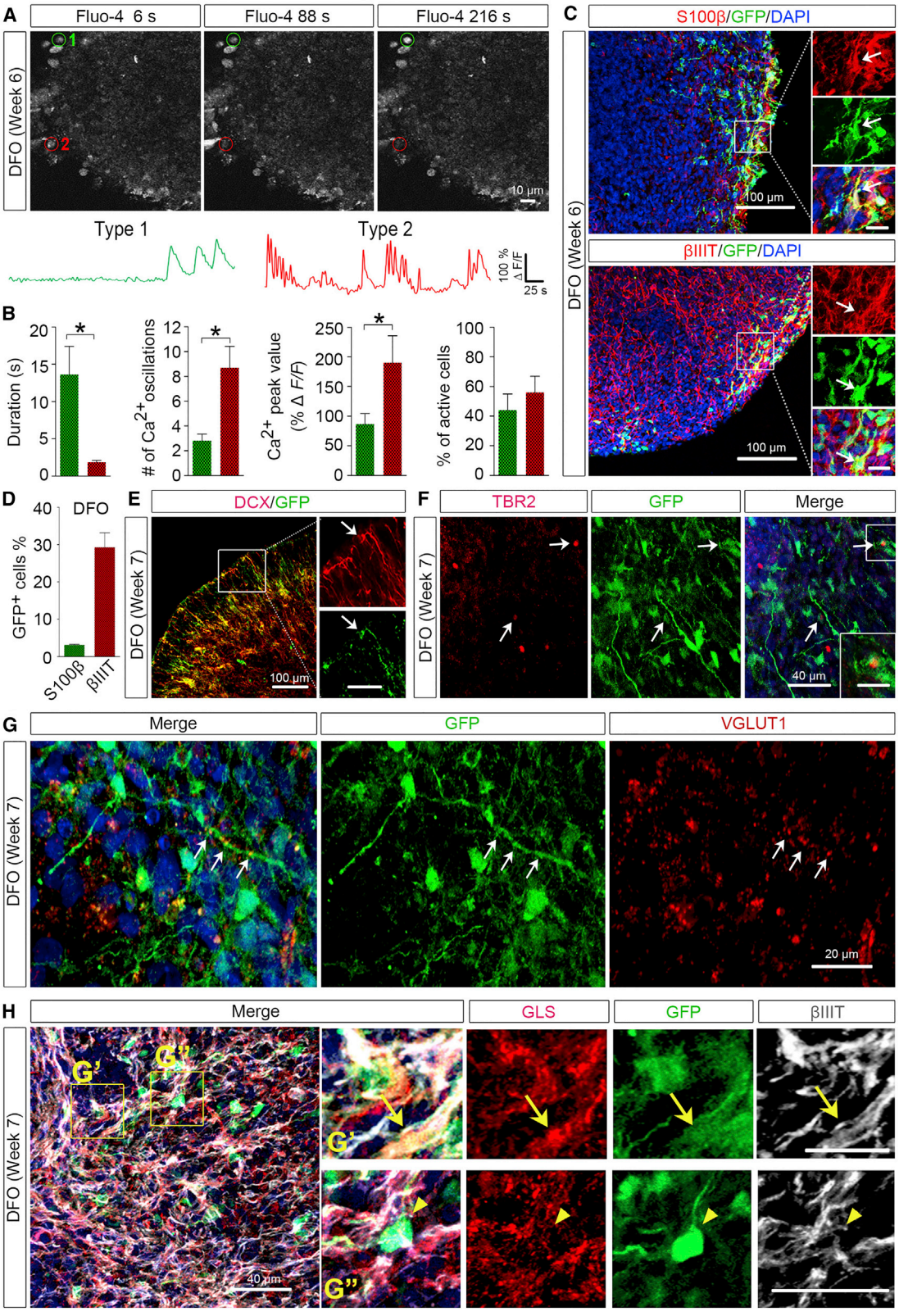


*(legend on next page)*

higher abundance of OLIG2$^+$ cells in VFOs than in DFOs. Notably, unlike the nuclear localization of OLIG2 in VFOs, GFP$^+$ cells in DFOs exhibited cytoplasmic OLIG2 expression (Figures 2A and 2C). Immunoblot analysis confirmed that OLIG2 was abundantly present in the nuclear fraction of VFOs, whereas OLIG2 was detected at a low level only in the cytoplasmic fraction of DFOs (Figure 2D). In the VFOs, nearly all GFP$^+$ cells expressed NKX2.1 (Figure 2E). As predicted, there were virtually no detectable NKX2.1$^+$ cells in the DFOs (Figures 1D and 1E). A subpopulation of GFP$^+$ cells in the DFOs was co-localized with PAX6 staining (31.0% ± 1.6% of total GFP$^+$ cells), further indicating the dorsal forebrain identity of the OLIG2$^+$ cells in the DFOs (Figures 2E and 2F). Taken together, OLIG2 is not only expressed in the VFOs but also cytoplasmically expressed in a small subset of NPCs in the DFOs.

## OLIG2$^+$ NPCs with Dorsal Forebrain Regional Identity Can Give Rise to Glutamatergic Neurons

To further examine whether NPCs in the DFOs could differentiate into functional neurons and glial cells, we performed two-photon $Ca^{2+}$ imaging on the organoids at week 6. We recorded patterns of $Ca^{2+}$ transients from soma of total 78 spontaneously active cells collected from randomly selected five fields in two organoids. The $Ca^{2+}$ transients exhibited by astrocytes are slower transients, whereas the ones displayed by neurons are faster transients (Ohara et al., 2009; Tashiro et al., 2002). As shown in Figures 3A and 3B, based on the duration and the number of oscillations the patterns of $Ca^{2+}$ transients could be grouped into two types: type 1 "glia-like" cells that had a lower number of oscillations with longer durations (>10 s) and type 2 "neuron-like" cells that had a higher number of oscillations with shorter durations (<2 s). Type 2 "neuron-like" cells also exhibited a significantly higher peak value of $Ca^{2+}$ transients than type 1 "glia-like" cells (Figure 3B).

The nuclear localization of OLIG2 suggests differentiation to oligodendroglial lineage cells (Ligon et al., 2006), whereas cytoplasmic localization suggests differentiation to neuronal or astroglial cells (Setoguchi and Kondo, 2004; Takebayashi et al., 2000; Zhao et al., 2009). To delineate the identity of GFP$^+$ cells, we immunostained the organoids with astroglial marker S100β or neuronal marker βIIIT. As shown in Figure 3C, a large number of βIIIT$^+$ neurons and a small population of S100β$^+$ astrocytes were identified in 6-week-old DFOs. The GFP$^+$ NPCs in DFOs mainly differentiated into neurons with a small percentage giving rise to astroglia (Figure 3D). In addition, we double-stained the DFOs with GFP and DCX, a marker for migrating immature neurons (Gleeson et al., 1999), or TBR2, a marker for intermediate neuronal progenitors (Sessa et al., 2010). There were GFP$^+$/DCX$^+$ processes and some GFP$^+$ cells were positive for TBR2 (Figure 3E), further suggesting that these GFP$^+$/OLIG2$^+$ cells were able to differentiate to neuronal cells.

We also found the formation of glutamatergic synapses in week-7 DFOs, as indicated by the staining of VGLUT1$^+$ puncta (Figure 3G). Notably, some of the VGLUT1$^+$ puncta were found to distribute along the GFP$^+$ processes. This prompted us to further characterize the OLIG2$^+$ cells in the DFOs. We triple-stained the week-7 DFOs with GFP, βIIIT, and glutaminase (GLS), which is the enzyme essential for glutamate production in glutamatergic neurons and astrocytes in the brain (Aoki et al., 1991; Cardona et al., 2015). We found that a small population of GFP$^+$ neurons, marked by βIIIT, expressed GLS (Figure 3F), suggesting that the OLIG2$^+$/GFP$^+$ cells in the DFOs develop into glutamatergic neurons.

## BrainPhys Medium Promotes Neuronal Maturation in Both VFOs and DFOs

Mounting evidence suggests that neuronal maturation and activity influence oligodendrogenesis and myelination

**Figure 3. Neuronal Differentiation of OLIG2$^+$ cells in DFOs**

(A) Time-lapse images and representative traces of $Ca^{2+}$ transients in DFOs. Regions of interest of active fluo-4$^+$ cells are marked in red or green.

(B) Quantification of $Ca^{2+}$ transients. Scale bars represent 50 s and 100% $\Delta F/F$. Quantification for the number, peak value, and duration of the $Ca^{2+}$ transients (n = 5 fields from 2 organoids) are shown. Student's t test. *p < 0.05.

(C and D) Representatives (C) and quantification (D) of GFP$^+$/S100β$^+$ and GFP$^+$/βIIIT$^+$ cells among total GFP$^+$ cells (n = 3 organoids from two hPSC lines). Arrows in (C) indicate the GFP$^+$ cells that express S100β (upper panels) or βIIIT (lower panels). Scale bars, 100 μm in the original images and 20 μm in the enlarged images.

(E and F) Representative images showing co-localization of GFP with DCX (arrows, E) or TBR2 (arrows, F) in week-7 DFOs. Scale bars, 100 μm and 50 μm in the original and enlarged images, respectively, for DCX; 40 μm and 20 μm in the original and enlarged images, respectively, for TBR2.

(G) Representative images showing co-localization of VGLUT1 and GFP. Arrows indicate VGLUT1 puncta along a GFP$^+$ process. Scale bars, 20 μm.

(H) Representative images showing co-localization of GLS, GFP, and βIIIT in week-7 DFOs. Arrows indicate a GFP$^+$/βIIIT$^+$/GLS$^+$ neuron in the top panels of enlarged images, and arrowheads indicate a GFP$^+$ cell that was GLS-negative in the bottom panels of enlarged images. Scale bars, 80 μm (top panels) and 40 μm (bottom panels).

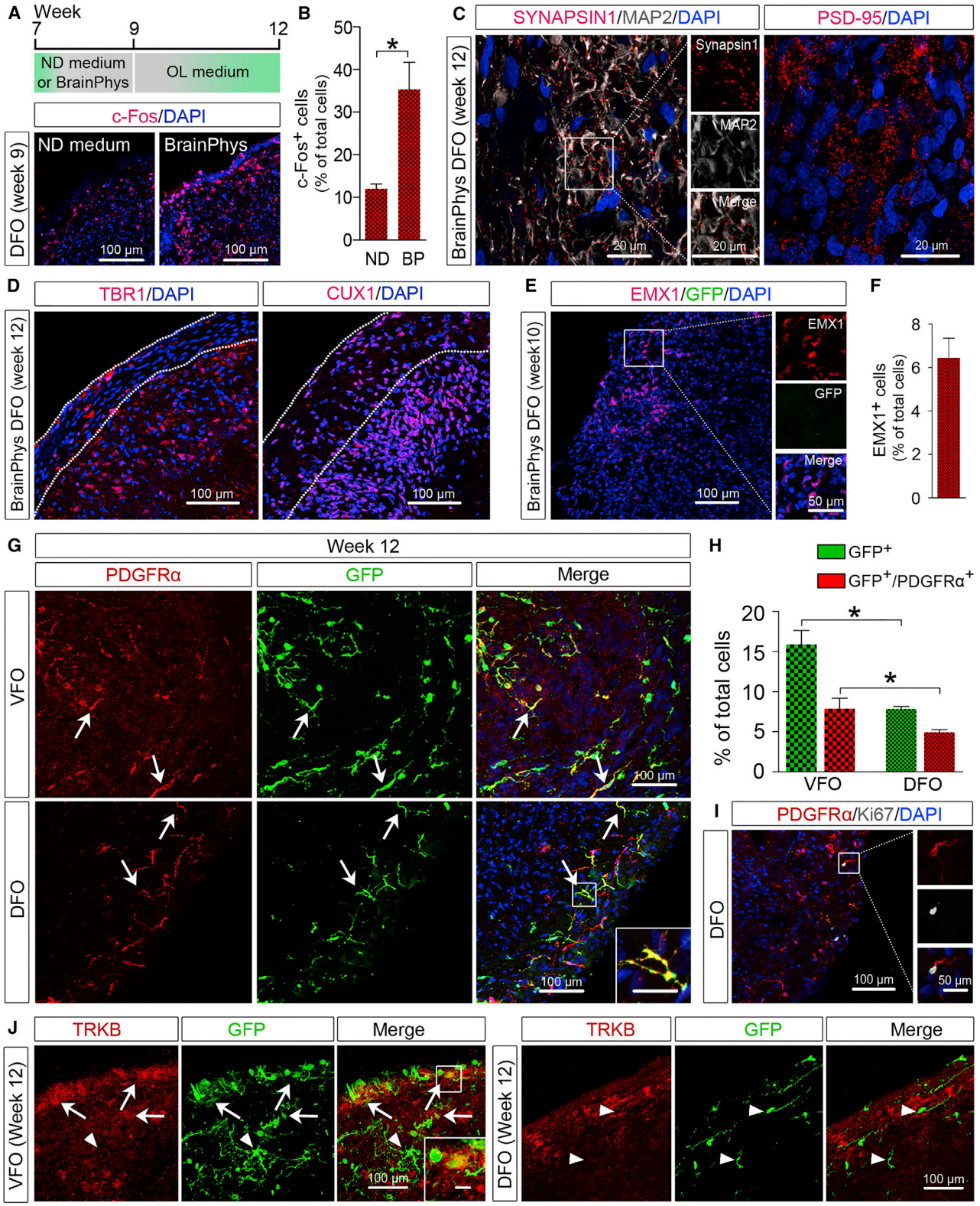


**Figure 4. Oligodendrogenesis in VFOs and DFOs after Neuronal Maturation Promoted by BrainPhys Medium**

(A and B) A schematic diagram and representatives (A), and quantification (B) of c-Fos$^+$ cells in week-9 DFOs cultured under different conditions (n = 4 organoids from two hPSC lines). Scale bar, 100 μm. Student's t test: *p < 0.05.

*(legend continued on next page)*

(Gibson et al., 2014; Mitew et al., 2018). A recent study developed a new BrainPhys medium to better support the neurophysiological activity of cultured human neurons (Bardy et al., 2015). We further cultured DFOs and VFOs in the BrainPhys medium from week 7 to week 9 (Figure 4A). We then examined the expression of c-Fos, an activity-dependent immediate-early gene that is expressed in neurons following depolarization and often used as a marker for mapping neuronal activity (Loebrich and Nedivi, 2009). As shown in Figures 4A and 4B, at week 9 there were significantly more c-Fos$^+$ cells in the organoids cultured in BrainPhys medium than in ND medium. Furthermore, we observed that the synaptic markers, PSD-95 and SYNAPSIN 1, were also expressed in the DFOs cultured in BrainPhys medium (Figure 4C). Moreover, neurons expressing CUX1, a marker for superficial-layer cortical neurons (Nieto et al., 2004) and TBR1$^+$, a marker for pre-plate/deep-layer neurons (Hevner et al., 2001), were also seen in the DFOs (Figure 4D). A small population of EMX1$^+$ dorsal NPCs was also found in DFOs (Figures 4E and 4F). At this time point, GFP signals became undetectable in the DFOs. In the VFOs, GFP fluorescence became much dimmer compared with week-7 VFOs (Figure 1G). This may result from the differentiation of a subset of OLIG2-expressing ventral forebrain NPCs to neurons, particularly interneurons (Xu et al., 2018), and subsequent termination of OLIG2/GFP expression in those cells, as reported in previous studies in mice (Miyoshi et al., 2007; Ono et al., 2008).

### Human PSC-Derived Organoids Reveal Oligodendrogenesis with Ventral and Dorsal Origins

To promote oligodendrogenesis in the DFOs and VFOs, we further cultured the organoids for an additional 3 weeks (Figure 4A; weeks 9–12) in OL differentiation medium containing thyroid hormone T3, which is commonly used to promote OL differentiation from hPSCs under 2D culture conditions (Goldman and Kuypers, 2015). As shown in Figure 1G, at week 12 there was a large number of bright GFP$^+$ cells evenly distributed in the VFOs. In the DFOs, GFP signal reappeared after the treatment of T3. To characterize the identity of these GFP$^+$ cells, we double-stained GFP with OPC marker platelet-derived growth factor receptor α (PDGFRα). In both VFOs and DFOs, nearly half of the GFP$^+$ expressed PDGFRα, indicating oligodendrogenesis in both organoids (Figures 4G and 4H). A subset of PDGFRα$^+$ OPCs in DFOs also exhibited immunoreactivity for Ki-67, suggesting that these OPCs were capable of proliferation (Figure 4I). In addition, we also stained the organoids with S100β or βIIIT, but found no GFP$^+$ cells expressing S100β or βIIIT at week 12. Thus, the GFP$^+$/PDGFRα$^-$ cells in the organoids might have committed to oligodendroglial fate but had not yet expressed any OPC marker. To further validate the ventral versus dorsal origin of the OPCs in VFOs and DFOs, we examined the expression of tyrosine kinase B (TRKB). Previous studies (Du et al., 2003) have shown that TRKB is selectively expressed in oligodendroglia from the basal forebrain that has a ventral origin (Kessaris et al., 2006; Klambt, 2009), but not in oligodendroglia from cerebral cortex that has a dorsal origin (Kessaris et al., 2006; Winkler et al., 2018). TRKB was robustly expressed by neurons in both VFOs and DFOs. Only a small population of TRKB$^+$/GFP$^+$ cells was seen in VFOs but no TRKB$^+$/GFP$^+$ cells in DFOs (Figure 4J). These results demonstrate that further culturing VFOs and DFOs under conditions favoring oligodendroglial differentiation can further reveal oligodendrogenesis with ventral and dorsal origins, respectively.

### OL Maturation in DFOs, VFOs, and Fused Forebrain Organoids

To examine whether OPCs in these organoids were able to mature into myelinating OLs, we cultured the VFOs and DFOs in OL medium for up to 6 weeks. Moreover, to test whether the interregional interactions between the differentially patterned human forebrain organoids are important for OL maturation, we generated FFOs and further cultured them in OL medium (Figure 5A). VFOs at week 5 were used for fusion with DFOs because previous studies showed that immature migrating interneurons generated by ventral forebrain NPCs promote OL formation in the cortex in a paracrine fashion (Voronova et al., 2017). After fusion, we observed a massive migration of GFP$^+$ cells from the VFOs into the DFOs (Figure 5B), similar to the observations reported in previous studies (Bagley et al., 2017; Birey et al., 2017; Xiang et al., 2017). At 3 weeks after fusion

(C) Representative images showing SYNAPSIN 1 and PSD-95 puncta in week-12 DFOs cultured in BrainPhys medium. Scale bar, 20 μm.
(D) Representative images showing TBR1$^+$ and CUX1$^+$ cells in week-12 DFOs cultured in BrainPhys medium. Scale bar, 100 μm.
(E and F) Representatives (E) and quantification (F) of EMX1$^+$ and GFP$^+$ cells in week-10 DFO culture in BrainPhys medium (n = 4 organoids from two hPSC lines). Scale bars, 100 μm in the original images and 50 μm in the enlarged images.
(G and H) Representatives (G) and quantification (H) of GFP$^+$ and PDGFRα$^+$ cells in week-12 VFOs and DFOs (n = 4 organoids from two hPSC lines). Arrows indicate the cells that are positive for PDGFRα and GFP. Student's t test: *p < 0.05. Scale bar, 100 μm.
(I) Representatives of PDGFRα$^+$/Ki-67$^+$ OPCs. Scale bars, 100 μm in the original images and 50 μm in the enlarged images.
(J) Representatives of TRKB- and GFP-expressing cells in VFOs and DFOs. Arrows indicate TRKB$^+$/GFP$^+$ cells. Arrowheads indicate TRKB$^-$/GFP$^+$ cells. Scale bars, 100 μm in the original images and 20 μm in the enlarged images.

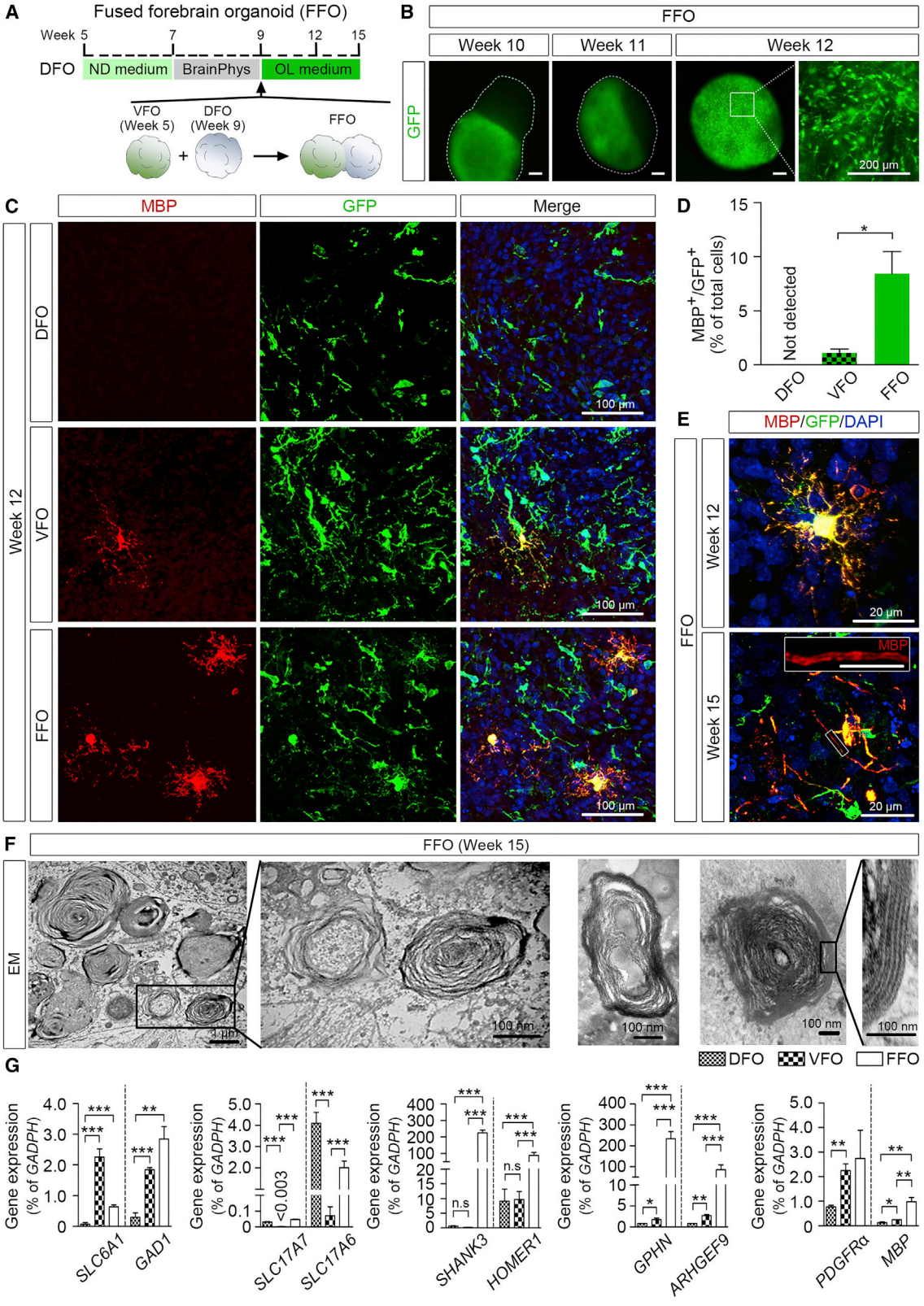


*(legend on next page)*

(week 12), GFP$^+$ cells largely populated the FFOs and exhibited bipolar morphology, characteristics of OPCs (Figure 5B). At week 15, we assessed OL maturation in DFOs, VFOs, and FFOs by staining myelin basic protein (MBP), a marker for mature OLs. As shown in Figures 5C and 5D, MBP$^+$/GFP$^+$ cells were detected in VFOs but not in DFOs. Interestingly, fusing the organoids significantly promoted the maturation of OLs, as indicated by a higher percentage of MBP$^+$/GFP$^+$ cells in FFOs. The mature OLs in FFOs exhibited complex processes at week 12 and occasionally we observed tubular-shaped MBP staining in FFOs at week 15 (Figure 5E), suggesting that the OLs started to myelinate axons. We further examined myelin ultrastructure in eight sections from four FFOs. In total, we identified 52 myelinated axons. As shown in Figure 5F, axons with loose escheatment by a few myelin laminae and some axons with compact myelin were observed in week-15 FFOs, which is similar to the "unorganized" myelin structure observed in oligocortical spheroids in a recent study (Madhavan et al., 2018) and also partly resembles the earliest stage of *in vivo* fetal myelinogenesis in humans (Weidenheim et al., 1992).

We next examined the gene expression of markers for excitatory and inhibitory neurons as well as markers for inhibitory and excitatory synapses in VFOs, DFOs, and FFOs. As shown in Figure 5G, the genes for markers of inhibitory neurons, including *SLC6A1* and *GAD1* that respectively encode γ-aminobutyric acid (GABA) transporter type 1 and glutamate decarboxylase 1, were expressed at much higher levels in VFOs than in DFOs. In contrast, genes for markers of excitatory neurons, including *SLC17A7* and *SLC17A6* that respectively encode vesicular glutamate transporters VGLUT1 and VGLUT2, were expressed at higher levels in DFOs than in VFOs. Importantly, FFOs exhibited well-balanced expression of all these gene transcripts compared with DFOs and VFOs. FFOs exhibited not only significantly enhanced expression of markers for inhibitory neurons compared with DFOs, but also enhanced expression of markers for excitatory neurons compared with VFOs. Furthermore, we examined the expression of genes for components of postsynaptic machinery, such as *HOMER1* and *SHANK3* that respectively encode excitatory postsynaptic components HOMER and SHANK, and *ARHGEF9* and *GPHN* that respectively encode inhibitory postsynaptic components COLLYBISTIN and GEPHYRIN. Compared with DFOs and VFOs, FFOs exhibited significantly enhanced expression of the genes for components of both inhibitory and excitatory postsynaptic. The expression of genes for inhibitory postsynaptic components was higher in VFOs than in DFOs, and the expression of genes for excitatory postsynaptic components was similar in VFOs and DFOs. These findings demonstrate that the FFOs generated in our study possess integrated glutamatergic and GABAergic neurons and have enhanced expression of synaptic markers, consistent with the results reported in recent studies (Birey et al., 2017; Xiang et al., 2017). Notably, the expression of *MBP* gene was also significantly higher in FFOs than in DFOs or VFOs. *PDGFRα* gene was expressed at a similar level in FFOs and VFOs, but at a lower level in DFOs. Our observation suggests that enhanced neuronal network in our organoids might contribute to OL differentiation and maturation.

## Dorsally Derived Oligodendroglia Outcompete Ventrally Derived Oligodendroglia in the FFOs

To further examine which population of oligodendroglia constituted the oligodendroglial cells in FFOs, we generated a new version of fused forebrain organoids by fusing the VFOs and DFOs that were respectively derived from isogenic OLIG2-GFP hiPSC reporter line and ND2.0 hiPSCs, which do not have any reporter fluorescence (Figure 6A). The isogenicity of OLIG2-GFP hiPSCs and ND2.0 hiPSCs were indicated by the identical short tandem repeat (STR) genotyping profile (Table S1). In addition, we did not observe any growth advantage on one line versus the other between the two iPSC lines. We then examined the interactions between ventrally and dorsally derived oligodendroglia in those FFOs. Since OLIG2 is expressed in all oligodendroglial lineage cells (Ligon et al., 2006), in this setting dorsally and ventrally derived oligodendroglia could be readily distinguished because the former would be GFP$^-$/OLIG2$^+$, whereas the latter would be GFP$^+$/OLIG2$^+$. As

**Figure 5. Oligodendroglial Maturation in DFOs, VFOs, and FFOs**

(A) A schematic procedure for fusing DFOs with VFOs and further culturing the FFOs in OL medium.

(B) Representatives of GFP expression during the fusion process. FFOs are outlined with dotted lines at weeks 10 and 11. Scale bars, 200 μm.

(C and D) Representatives (C) and quantification (D) of MBP$^+$/GFP$^+$ cells in VFOs, DFOs, and FFOs at week 12 (n = 4 organoids for each group). Student's t test: *p < 0.05. Scale bar, 100 μm.

(E) Representatives of MBP$^+$ cells in week-12 and week-15 FFOs. Scale bars, 20 μm in the original and images and 10 μm in the enlarged images.

(F) Representative electron microscopy images of the myelin ultrastructure in week-15 FFOs. Scale bars, 1 μm and 100 nm.

(G) qRT-PCR results showing the expression of *SLC6A1*, *GAD1*, *SLC17A7*, *SLC17A6*, *SHANK3*, *HOMER1*, *GPHN*, *ARHGEF9*, *PDGFRα*, and *MBP* in VFOs, DFOs, and FFOs (n = 3 independent experiments). One-way ANOVA with Tukey's post hoc test: *p < 0.05, **p < 0.01, ***p < 0.001.

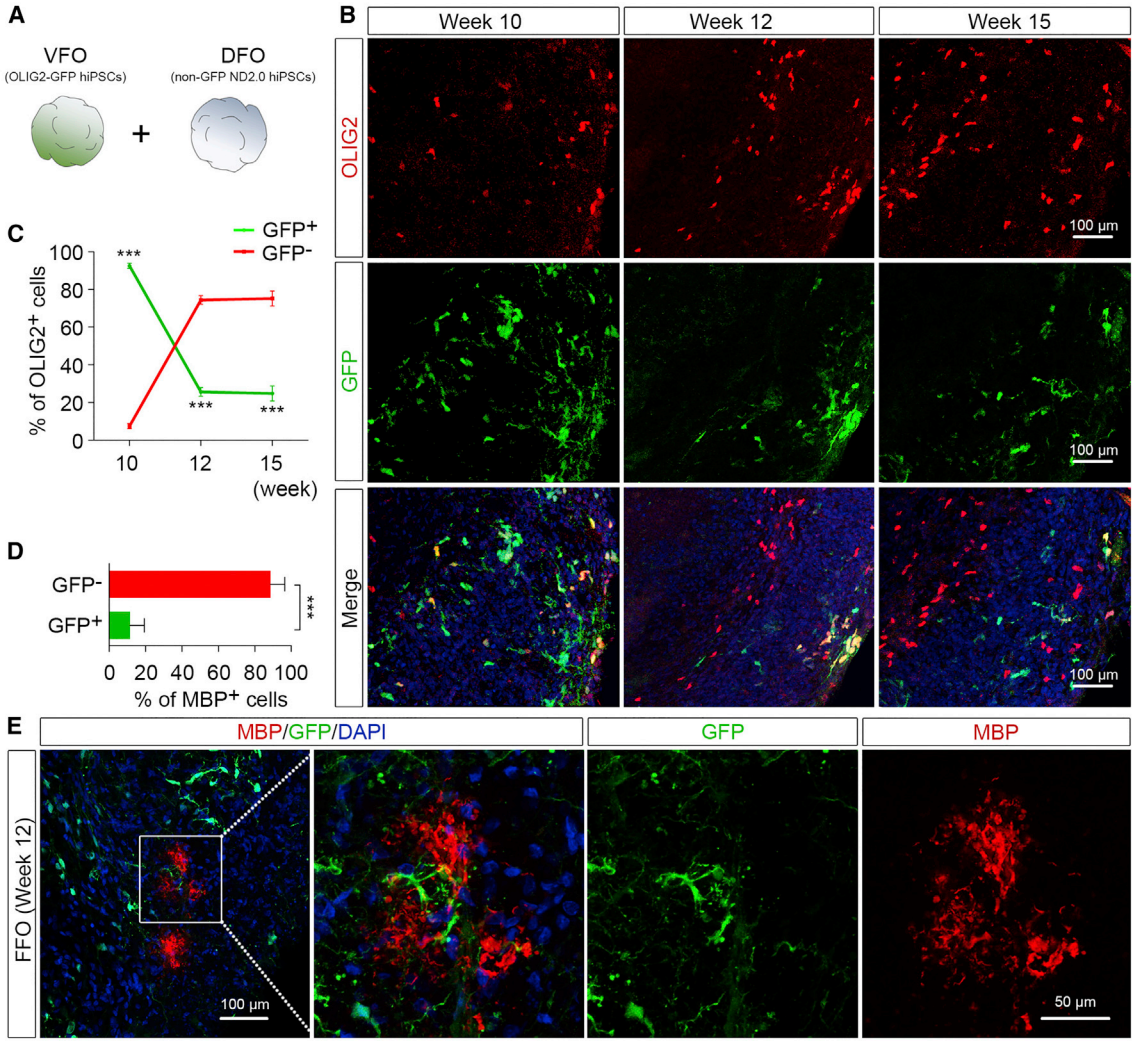


**Figure 6. Interactions between Dorsally and Ventrally Derived Oligodendroglia in the FFOs**

(A) A schematic procedure for fusing the VFOs and DFOs that were respectively derived from isogenic OLIG2-GFP hiPSC reporter line and ND2.0 hiPSC line that do not have any reporter fluorescence.

(B and C) Representatives (B) and quantification (C) (n = 4 organoids) showing that ventrally derived OLIG2$^+$ cells (GFP$^+$) are outnumbered by dorsally derived OLIG2$^+$ cells (GFP-negative) at 1 week after fusion (week 10) to 6 weeks after fusion (week 15). Student's t test: ***p < 0.001. Scale bar, 100 μm.

(D and E) Quantification (D) and representatives (E) showing MBP$^+$ cells with a ventral (GFP$^+$) or dorsal (GFP-negative) origin (n = 4 organoids). Student's t test: ***p < 0.001. Scale bars, 50 μm.

shown in Figures 6B and 6C, at 1 week after fusion (week 10), the ventrally derived GFP$^+$/OLIG2$^+$ cells outnumbered the dorsally derived GFP$^-$/OLIG2$^+$ cells. At 3 and 6 weeks after fusion (weeks 12 and 15), the dorsally derived GFP$^-$/OLIG2$^+$ cells became a dominant population, whereas the ventrally derived GFP$^+$/OLIG2$^+$ cells dramatically decreased in the FFOs from week 10 to week 15 (Figures 6B and 6C). Furthermore, at week 12 the majority of MBP$^+$ cells were MBP$^+$/GFP$^-$ (Figures 6D and 6E), suggesting that those mature OLs had a dorsal origin. Taken together, these results demonstrate that the majority of oligodendroglia in the FFOs at an early stage (week 10) are ventrally derived oligodendroglia, which are outcompeted by dorsally derived oligodendroglia in the FFOs at later stages (weeks 12 and 15).

## DISCUSSION

OLIG2 is not only closely associated with the development of OLs in the vertebrate CNS but also is expressed in NPCs during development (Jiang et al., 2013; Ligon et al., 2006;

Meijer et al., 2012; Ono et al., 2008). At early embryonic stages in mice, OLIG2 is mostly expressed in the brain by the NPCs that distribute in the ventral telencephalon (Ligon et al., 2006; Meijer et al., 2012). A distinct but small number of OLIG2$^+$ NPCs that distribute in the dorsal forebrain has been also identified in both mouse and human embryonic brain (Jakovcevski and Zecevic, 2005; Ono et al., 2008). The small population of human OLIG2$^+$/PAX6$^+$ NPCs seen in the week-5 DFOs may mimic the OLIG2$^+$ NPCs in the human embryonic diencephalon (Jakovcevski and Zecevic, 2005). Furthermore, we demonstrate that these early human OLIG2$^+$ NPCs are also able to give rise to glutamatergic neurons and astrocytes in the organoids, similar to that seen in the mouse brain (Ono et al., 2008).

Interestingly, we revealed oligodendrogenesis with a dorsal origin in our organoid models. This oligodendrogenesis in DFOs likely recapitulates the third wave of oligodendrogenesis, firstly because these oligodendroglial cells are dorsally derived. The DFOs are generated by using pNPCs as the starting population, since these neural fate-restricted pNPCs retain high responsiveness to instructive neural patterning cues (Li et al., 2011) and can be efficiently patterned to desired brain regions (Monzel et al., 2017). We further enhanced the dorsalization using cyclopamine (Bagley et al., 2017; Vazin et al., 2014). In addition, we did not observe any ventral forebrain NPCs in DFOs. Second, these oligodendroglial cells are derived from progenitors that are distinct from the early OLIG2$^+$/PAX6$^+$ progenitor cells. At week 9, all OLIG2$^+$/PAX6$^+$ NPCs differentiate to neurons or astrocytes, and OLIG2 expression terminates as indicated by GFP fluorescence and qPCR results. Moreover, we find EMX1$^+$ dorsal forebrain NPCs in the 9-week-old organoids. It is very likely that those EMX1$^+$ cells further differentiate to oligodendroglial cells, similar to the findings in the mouse brain (Kessaris et al., 2006; Winkler et al., 2018). Third, the newly emerged OLIG2$^+$/PDGFR$\alpha^+$ cells in week-12 DFOs are able to proliferate and populate the organoids, indicating their OPC nature. Lastly, these dorsally derived oligodendroglia can outcompete ventrally derived oligodendroglia in the FFOs, which may mimic the process of oligodendrogenesis in the cerebral cortex, where ventrally derived oligodendroglia are outcompeted by oligodendroglia with a dorsal origin at late developmental stages (Kessaris et al., 2006). Thus, these results suggest that a dorsal origin of oligodendrogenesis may occur during human brain development.

Technically, we also develop organoid models with significantly accelerated OL maturation. Deriving mature OLs from human PSCs is a tedious and lengthy process, and optimizing methods to obtain human mature OLs has been a major research effort (Douvaras and Fossati, 2015; Goldman and Kuypers, 2015; Liu et al., 2011; Stacpoole et al., 2013). In our system, MBP$^+$ mature OLs appeared at 9 weeks after organoid formation. This acceleration of the OL maturation program in our organoids is likely achieved by promoting neuronal maturation with the newly designed BrainPhys medium and rebuilding the neuronal network in FFOs. Balanced excitatory and inhibitory neuronal activities (Nagy et al., 2017), neurotransmitters and neurotrophins released by excitatory neurons or astrocytes (Gautier et al., 2015; Lundgaard et al., 2013; Xiao et al., 2009), and cytokines released by young migrating inhibitory neurons (Voronova et al., 2017) may partly contribute to the enhanced oligodendroglial lineage progression in FFOs. Compared with the fusion methods, generating a single, regionalized organoids containing both ventral and dorsal elements (Cederquist et al., 2019) may more precisely recapitulate the serial waves of oligodendroglial production and replacement seen in the developing forebrain, because the different germinal zones within single organoids might be well preserved and not be disrupted by the fusion process. Notably, similar to recent studies (Madhavan et al., 2018; Marton et al., 2019), the maturation of human OPCs is not efficient in organoids, and those myelinated axons often show wrapping with multiple layers of uncompacted myelin. This may be attributed in part to a lack of oxygen penetration in the organoids cultured for the long term, which can result in necrosis in the core of organoids (Brawner et al., 2017; Giandomenico and Lancaster, 2017). As opposed to rodent OPCs, human OPC differentiation and myelination are highly sensitive to hypoxic conditions (Gautier et al., 2015). Future studies aiming at integrating a vascular structure that brings adequate delivery of oxygen and nutrients and promotes neuronal maturation and electrical activity (Brawner et al., 2017; Mansour et al., 2018) may help facilitate organoid models with robust OL maturation.

Previous *in vivo* studies have helped us understand the developmental differences between ventrally and dorsally derived OPCs (Kessaris et al., 2006; Nery et al., 2001; Orentas et al., 1999; Winkler et al., 2018). However, the phenotypic and functional differences between the different populations of OPCs are largely unclear. In this study, we demonstrate the generation of dorsally and ventrally derived human oligodendroglial cells in organoids. We propose that the competitive advantage exhibited by dorsally derived over ventrally derived OPCs may partly result from their unique expression pattern of molecules involved in controlling OPC proliferation and lineage progression, for example GPR17, a G-protein-coupled membrane receptor suggested as an intrinsic timer of OL differentiation during development (Chen et al., 2009; Fumagalli et al., 2011), and transcription factor EB, which recently has been identified to govern the regional and temporal specificity of OL differentiation and myelination (Sun et al., 2018). Future

gene-expression profiling at a single-cell level in the separate dorsal and VFOs as well as FFOs will significantly advance our understanding of the heterogeneity of human OPCs. In combination with human iPSC technologies, examining oligodendroglia in region-specific organoids may be more informative for understanding disease mechanisms of neurodevelopmental disorders associated with myelin defects. These organoid models could also have important implications in the setting of CNS injury, as distinct populations of human OPCs might respond to promyelinating drugs differently, preferentially contributing to remyelination, thus enabling a better model for therapeutic manipulation.

## EXPERIMENTAL PROCEDURES

For further details, see Supplemental Experimental Procedures.

### Generation of Human Forebrain Organoids with hPSC Lines

All the hPSC studies were approved by the committees on stem cell research at Rutgers University. Forebrain organoids differentiation was carried out as previously reported (Bagley et al., 2017; Birey et al., 2017; Xiang et al., 2017) with modifications.

### qRT-PCR

Gene expressions were measured by performing qRT-PCR with TaqMan primers listed in Table S2.

### Western Blotting

Protein expression and localization in cells were evaluated by immunoblotting with samples achieved by the REAP method (Suzuki et al., 2010).

### Immunostaining

Fixed organoids were processed for immunostaining with primary antibodies listed in Table S3.

### Calcium Imaging

DFOs loaded with fluo-4 AM (5 μM, Molecular Probes) was performed with a two-photon microscope (Moving Objective Microscope; Sutter Instruments).

### Electron Microscopy

Selected vibratome sections from organoid samples were used for electron microscopy.

### DNA Fingerprinting Short Tandem Repeat Analysis

GENEprint PowerPlex 16 kit (Promega performed by Cell Line Genetics. LLC) was used for STR analysis.

### Statistical Analysis

All experiments were repeated at least three times ($n \geq 3$). Unless otherwise noted, organoids derived from OLIG2-GFP hESCs and hiPSCs were analyzed for each experiment. Data are presented as mean ± SEM and were analyzed using one-way ANOVA in combination with Tukey's post hoc test or Student's t test. For statistical significance, p values of $<0.05$ were considered significant.

## SUPPLEMENTAL INFORMATION

Supplemental Information can be found online at https://doi.org/10.1016/j.stemcr.2019.04.011.

## AUTHOR CONTRIBUTIONS

H.K. and P.J. designed experiments and interpreted data; H.K. carried out most of experiments with technical assistance from R.X.; R.P. and A.D. performed calcium imaging experiments; Y.L. and C.F.D. provided study materials and reagents and provided critical suggestions to the overall research direction. P.J. directed the project and wrote the manuscript together with H.K. and input from all co-authors.

## ACKNOWLEDGMENTS

This work was in part supported by grants from the NIH (R21HD091512 and R01NS102382 to P.J.) and a pilot grant from Rutgers Brain Health Institute to P.J.

Received: July 11, 2018
Revised: April 8, 2019
Accepted: April 9, 2019
Published: May 14, 2019

## REFERENCES

Aoki, C., Kaneko, T., Starr, A., and Pickel, V.M. (1991). Identification of mitochondrial and non-mitochondrial glutaminase within select neurons and glia of rat forebrain by electron microscopic immunocytochemistry. J. Neurosci. Res. *28*, 531–548.

Avior, Y., Sagi, I., and Benvenisty, N. (2016). Pluripotent stem cells in disease modelling and drug discovery. Nat. Rev. Mol. Cell Biol. *17*, 170–182.

Bagley, J.A., Reumann, D., Bian, S., Levi-Strauss, J., and Knoblich, J.A. (2017). Fused cerebral organoids model interactions between brain regions. Nat. Methods *14*, 743–751.

Bardy, C., van den Hurk, M., Eames, T., Marchand, C., Hernandez, R.V., Kellogg, M., Gorris, M., Galet, B., Palomares, V., Brown, J., et al. (2015). Neuronal medium that supports basic synaptic functions and activity of human neurons in vitro. Proc. Natl. Acad. Sci. U S A *112*, E2725–E2734.

Birey, F., Andersen, J., Makinson, C.D., Islam, S., Wei, W., Huber, N., Fan, H.C., Metzler, K.R.C., Panagiotakos, G., Thom, N., et al. (2017). Assembly of functionally integrated human forebrain spheroids. Nature *545*, 54–59.

Brawner, A.T., Xu, R., Liu, D., and Jiang, P. (2017). Generating CNS organoids from human induced pluripotent stem cells for modeling neurological disorders. Int. J. Physiol. Pathophysiol. Pharmacol. *9*, 101–111.

Briscoe, J., Sussel, L., Serup, P., Hartigan-O'Connor, D., Jessell, T.M., Rubenstein, J.L., and Ericson, J. (1999). Homeobox gene Nkx2.2

and specification of neuronal identity by graded Sonic hedgehog signalling. Nature *398*, 622–627.

Cardona, C., Sanchez-Mejias, E., Davila, J.C., Martin-Rufian, M., Campos-Sandoval, J.A., Vitorica, J., Alonso, F.J., Mates, J.M., Segura, J.A., Norenberg, M.D., et al. (2015). Expression of Gls and Gls2 glutaminase isoforms in astrocytes. Glia *63*, 365–382.

Cederquist, G.Y., Asciolla, J.J., Tchieu, J., Walsh, R.M., Cornacchia, D., Resh, M.D., and Studer, L. (2019). Specification of positional identity in forebrain organoids. Nat. Biotechnol. *37*, 436–444.

Chapman, H., Waclaw, R.R., Pei, Z., Nakafuku, M., and Campbell, K. (2013). The homeobox gene Gsx2 controls the timing of oligodendroglial fate specification in mouse lateral ganglionic eminence progenitors. Development *140*, 2289–2298.

Chen, Y., Wu, H., Wang, S., Koito, H., Li, J., Ye, F., Hoang, J., Escobar, S.S., Gow, A., Arnett, H.A., et al. (2009). The oligodendrocyte-specific G protein-coupled receptor GPR17 is a cell-intrinsic timer of myelination. Nat. Neurosci. *12*, 1398–1406.

Douvaras, P., and Fossati, V. (2015). Generation and isolation of oligodendrocyte progenitor cells from human pluripotent stem cells. Nat. Protoc. *10*, 1143–1154.

Du, Y., Fischer, T.Z., Lee, L.N., Lercher, L.D., and Dreyfus, C.F. (2003). Regionally specific effects of BDNF on oligodendrocytes. Dev. Neurosci. *25*, 116–126.

Du, T., Xu, Q., Ocbina, P.J., and Anderson, S.A. (2008). NKX2.1 specifies cortical interneuron fate by activating Lhx6. Development *135*, 1559–1567.

Englund, C., Fink, A., Lau, C., Pham, D., Daza, R.A., Bulfone, A., Kowalczyk, T., and Hevner, R.F. (2005). Pax6, Tbr2, and Tbr1 are expressed sequentially by radial glia, intermediate progenitor cells, and postmitotic neurons in developing neocortex. J. Neurosci. *25*, 247–251.

Fumagalli, M., Daniele, S., Lecca, D., Lee, P.R., Parravicini, C., Fields, R.D., Rosa, P., Antonucci, F., Verderio, C., Trincavelli, M.L., et al. (2011). Phenotypic changes, signaling pathway, and functional correlates of GPR17-expressing neural precursor cells during oligodendrocyte differentiation. J. Biol. Chem. *286*, 10593–10604.

Gautier, H.O., Evans, K.A., Volbracht, K., James, R., Sitnikov, S., Lundgaard, I., James, F., Lao-Peregrin, C., Reynolds, R., Franklin, R.J., et al. (2015). Neuronal activity regulates remyelination via glutamate signalling to oligodendrocyte progenitors. Nat. Commun. *6*, 8518.

Giandomenico, S.L., and Lancaster, M.A. (2017). Probing human brain evolution and development in organoids. Curr. Opin. Cell Biol. *44*, 36–43.

Gibson, E.M., Purger, D., Mount, C.W., Goldstein, A.K., Lin, G.L., Wood, L.S., Inema, I., Miller, S.E., Bieri, G., Zuchero, J.B., et al. (2014). Neuronal activity promotes oligodendrogenesis and adaptive myelination in the mammalian brain. Science *344*, 1252304.

Gleeson, J.G., Lin, P.T., Flanagan, L.A., and Walsh, C.A. (1999). Doublecortin is a microtubule-associated protein and is expressed widely by migrating neurons. Neuron *23*, 257–271.

Goldman, S.A., and Kuypers, N.J. (2015). How to make an oligodendrocyte. Development *142*, 3983–3995.

Gorski, J.A., Talley, T., Qiu, M., Puelles, L., Rubenstein, J.L., and Jones, K.R. (2002). Cortical excitatory neurons and glia, but not GABAergic neurons, are produced in the Emx1-expressing lineage. J. Neurosci. *22*, 6309–6314.

Hevner, R.F., Shi, L., Justice, N., Hsueh, Y., Sheng, M., Smiga, S., Bulfone, A., Goffinet, A.M., Campagnoni, A.T., and Rubenstein, J.L. (2001). Tbr1 regulates differentiation of the preplate and layer 6. Neuron *29*, 353–366.

Jakovcevski, I., and Zecevic, N. (2005). Olig transcription factors are expressed in oligodendrocyte and neuronal cells in human fetal CNS. J. Neurosci. *25*, 10064–10073.

Jakovcevski, I., Filipovic, R., Mo, Z., Rakic, S., and Zecevic, N. (2009). Oligodendrocyte development and the onset of myelination in the human fetal brain. Front. Neuroanat. *3*, 5.

Jiang, P., Chen, C., Wang, R., Chechneva, O.V., Chung, S.H., Rao, M.S., Pleasure, D.E., Liu, Y., Zhang, Q., and Deng, W. (2013). hESC-derived Olig2+ progenitors generate a subtype of astroglia with protective effects against ischaemic brain injury. Nat. Commun. *4*, 2196.

Kessaris, N., Fogarty, M., Iannarelli, P., Grist, M., Wegner, M., and Richardson, W.D. (2006). Competing waves of oligodendrocytes in the forebrain and postnatal elimination of an embryonic lineage. Nat. Neurosci. *9*, 173–179.

Klambt, C. (2009). Modes and regulation of glial migration in vertebrates and invertebrates. Nat. Rev. Neurosci. *10*, 769–779.

Li, W., Sun, W., Zhang, Y., Wei, W., Ambasudhan, R., Xia, P., Talantova, M., Lin, T., Kim, J., Wang, X., et al. (2011). Rapid induction and long-term self-renewal of primitive neural precursors from human embryonic stem cells by small molecule inhibitors. Proc. Natl. Acad. Sci. U S A *108*, 8299–8304.

Ligon, K.L., Fancy, S.P., Franklin, R.J., and Rowitch, D.H. (2006). Olig gene function in CNS development and disease. Glia *54*, 1–10.

Liu, Y., Jiang, P., and Deng, W. (2011). OLIG gene targeting in human pluripotent stem cells for motor neuron and oligodendrocyte differentiation. Nat. Protoc. *6*, 640–655.

Loebrich, S., and Nedivi, E. (2009). The function of activity-regulated genes in the nervous system. Physiol. Rev. *89*, 1079–1103.

Lundgaard, I., Luzhynskaya, A., Stockley, J.H., Wang, Z., Evans, K.A., Swire, M., Volbracht, K., Gautier, H.O., Franklin, R.J., Charles, F.-C., et al. (2013). Neuregulin and BDNF induce a switch to NMDA receptor-dependent myelination by oligodendrocytes. PLoS Biol. *11*, e1001743.

Madhavan, M., Nevin, Z.S., Shick, H.E., Garrison, E., Clarkson-Paredes, C., Karl, M., Clayton, B.L.L., Factor, D.C., Allan, K.C., Barbar, L., et al. (2018). Induction of myelinating oligodendrocytes in human cortical spheroids. Nat. Methods *15*, 700–706.

Mansour, A.A., Goncalves, J.T., Bloyd, C.W., Li, H., Fernandes, S., Quang, D., Johnston, S., Parylak, S.L., Jin, X., and Gage, F.H. (2018). An in vivo model of functional and vascularized human brain organoids. Nat. Biotechnol. *36*, 432–441.

Marchetto, M.C., Brennand, K.J., Boyer, L.F., and Gage, F.H. (2011). Induced pluripotent stem cells (iPSCs) and neurological disease modeling: progress and promises. Hum. Mol. Genet. *20*, R109–R115.

Marton, R.M., Miura, Y., Sloan, S.A., Li, Q., Revah, O., Levy, R.J., Huguenard, J.R., and Pasca, S.P. (2019). Differentiation and

maturation of oligodendrocytes in human three-dimensional neural cultures. Nat. Neurosci. *22*, 484–491.

Meijer, D.H., Kane, M.F., Mehta, S., Liu, H., Harrington, E., Taylor, C.M., Stiles, C.D., and Rowitch, D.H. (2012). Separated at birth? The functional and molecular divergence of OLIG1 and OLIG2. Nat. Rev. Neurosci. *13*, 819–831.

Mitew, S., Gobius, I., Fenlon, L.R., McDougall, S.J., Hawkes, D., Xing, Y.L., Bujalka, H., Gundlach, A.L., Richards, L.J., Kilpatrick, T.J., et al. (2018). Pharmacogenetic stimulation of neuronal activity increases myelination in an axon-specific manner. Nat. Commun. *9*, 306.

Miyoshi, G., Butt, S.J., Takebayashi, H., and Fishell, G. (2007). Physiologically distinct temporal cohorts of cortical interneurons arise from telencephalic Olig2-expressing precursors. J. Neurosci. *27*, 7786–7798.

Monzel, A.S., Smits, L.M., Hemmer, K., Hachi, S., Moreno, E.L., van Wuellen, T., Jarazo, J., Walter, J., Bruggemann, I., Boussaad, I., et al. (2017). Derivation of human midbrain-specific organoids from neuroepithelial stem cells. Stem Cell Reports *8*, 1144–1154.

Nagy, B., Hovhannisyan, A., Barzan, R., Chen, T.J., and Kukley, M. (2017). Different patterns of neuronal activity trigger distinct responses of oligodendrocyte precursor cells in the corpus callosum. PLoS Biol. *15*, e2001993.

Nery, S., Wichterle, H., and Fishell, G. (2001). Sonic hedgehog contributes to oligodendrocyte specification in the mammalian forebrain. Development *128*, 527–540.

Nieto, M., Monuki, E.S., Tang, H., Imitola, J., Haubst, N., Khoury, S.J., Cunningham, J., Gotz, M., and Walsh, C.A. (2004). Expression of Cux-1 and Cux-2 in the subventricular zone and upper layers II-IV of the cerebral cortex. J. Comp. Neurol. *479*, 168–180.

Ohara, P.T., Vit, J.P., Bhargava, A., Romero, M., Sundberg, C., Charles, A.C., and Jasmin, L. (2009). Gliopathic pain: when satellite glial cells go bad. Neuroscientist *15*, 450–463.

Ono, K., Takebayashi, H., Ikeda, K., Furusho, M., Nishizawa, T., Watanabe, K., and Ikenaka, K. (2008). Regional- and temporal-dependent changes in the differentiation of Olig2 progenitors in the forebrain, and the impact on astrocyte development in the dorsal pallium. Dev. Biol. *320*, 456–468.

Orentas, D.M., Hayes, J.E., Dyer, K.L., and Miller, R.H. (1999). Sonic hedgehog signaling is required during the appearance of spinal cord oligodendrocyte precursors. Development *126*, 2419–2429.

Pasca, S.P. (2018). The rise of three-dimensional human brain cultures. Nature *553*, 437–445.

Petryniak, M.A., Potter, G.B., Rowitch, D.H., and Rubenstein, J.L. (2007). Dlx1 and Dlx2 control neuronal versus oligodendroglial cell fate acquisition in the developing forebrain. Neuron *55*, 417–433.

Rakic, S., and Zecevic, N. (2003). Early oligodendrocyte progenitor cells in the human fetal telencephalon. Glia *41*, 117–127.

Sessa, A., Mao, C.A., Colasante, G., Nini, A., Klein, W.H., and Broccoli, V. (2010). Tbr2-positive intermediate (basal) neuronal progenitors safeguard cerebral cortex expansion by controlling amplification of pallial glutamatergic neurons and attraction of subpallial GABAergic interneurons. Genes Dev. *24*, 1816–1826.

Setoguchi, T., and Kondo, T. (2004). Nuclear export of OLIG2 in neural stem cells is essential for ciliary neurotrophic factor-induced astrocyte differentiation. J. Cell Biol. *166*, 963–968.

Stacpoole, S.R., Spitzer, S., Bilican, B., Compston, A., Karadottir, R., Chandran, S., and Franklin, R.J. (2013). High yields of oligodendrocyte lineage cells from human embryonic stem cells at physiological oxygen tensions for evaluation of translational biology. Stem Cell Reports *1*, 437–450.

Sun, L.O., Mulinyawe, S.B., Collins, H.Y., Ibrahim, A., Li, Q., Simon, D.J., Tessier-Lavigne, M., and Barres, B.A. (2018). Spatiotemporal control of CNS myelination by oligodendrocyte programmed cell death through the TFEB-PUMA Axis. Cell *175*, 1811–1826.e21.

Suzuki, K., Bose, P., Leong-Quong, R.Y., Fujita, D.J., and Riabowol, K. (2010). REAP: a two minute cell fractionation method. BMC Res. Notes *3*, 294.

Takebayashi, H., Yoshida, S., Sugimori, M., Kosako, H., Kominami, R., Nakafuku, M., and Nabeshima, Y. (2000). Dynamic expression of basic helix-loop-helix Olig family members: implication of Olig2 in neuron and oligodendrocyte differentiation and identification of a new member, Olig3. Mech. Dev. *99*, 143–148.

Tao, Y., and Zhang, S.C. (2016). Neural subtype specification from human pluripotent stem cells. Cell Stem Cell *19*, 573–586.

Tashiro, A., Goldberg, J., and Yuste, R. (2002). Calcium oscillations in neocortical astrocytes under epileptiform conditions. J. Neurobiol. *50*, 45–55.

Tekki-Kessaris, N., Woodruff, R., Hall, A.C., Gaffield, W., Kimura, S., Stiles, C.D., Rowitch, D.H., and Richardson, W.D. (2001). Hedgehog-dependent oligodendrocyte lineage specification in the telencephalon. Development *128*, 2545–2554.

Tripathi, R.B., Clarke, L.E., Burzomato, V., Kessaris, N., Anderson, P.N., Attwell, D., and Richardson, W.D. (2011). Dorsally and ventrally derived oligodendrocytes have similar electrical properties but myelinate preferred tracts. J. Neurosci. *31*, 6809–6819.

Vazin, T., Ball, K.A., Lu, H., Park, H., Ataeijannati, Y., Head-Gordon, T., Poo, M.M., and Schaffer, D.V. (2014). Efficient derivation of cortical glutamatergic neurons from human pluripotent stem cells: a model system to study neurotoxicity in Alzheimer's disease. Neurobiol. Dis. *62*, 62–72.

Voronova, A., Yuzwa, S.A., Wang, B.S., Zahr, S., Syal, C., Wang, J., Kaplan, D.R., and Miller, F.D. (2017). Migrating interneurons secrete fractalkine to promote oligodendrocyte formation in the developing mammalian brain. Neuron *94*, 500–516.e9.

Weidenheim, K.M., Kress, Y., Epshteyn, I., Rashbaum, W.K., and Lyman, W.D. (1992). Early myelination in the human fetal lumbosacral spinal cord: characterization by light and electron microscopy. J. Neuropathol. Exp. Neurol. *51*, 142–149.

Winkler, C.C., Yabut, O.R., Fregoso, S.P., Gomez, H.G., Dwyer, B.E., Pleasure, S.J., and Franco, S.J. (2018). The dorsal wave of neocortical oligodendrogenesis begins embryonically and requires multiple sources of Sonic Hedgehog. J. Neurosci. *38*, 5237–5250.

Xiang, Y., Tanaka, Y., Patterson, B., Kang, Y.J., Govindaiah, G., Roselaar, N., Cakir, B., Kim, K.Y., Lombroso, A.P., Hwang, S.M., et al. (2017). Fusion of regionally specified hPSC-derived organoids

models human brain development and interneuron migration. Cell Stem Cell *21*, 383–398.e7.

Xiao, J., Kilpatrick, T.J., and Murray, S.S. (2009). The role of neurotrophins in the regulation of myelin development. Neurosignals *17*, 265–276.

Xu, R., Brawner, A., Li, S., Liu, J., Kim, H., Xue, H., Pang, Z., Kim, W.-Y., Hart, R., Liu, Y., et al. (2018). Reversing abnormal neural development by inhibiting OLIG2 in down syndrome human iPSC brain organoids and neuronal mouse chimeras. bioRxiv https://doi.org/10.1101/462739.

Xue, H., Wu, S., Papadeas, S.T., Spusta, S., Swistowska, A.M., MacArthur, C.C., Mattson, M.P., Maragakis, N.J., Capecchi, M.R., Rao, M.S., et al. (2009). A targeted neuroglial reporter line generated by homologous recombination in human embryonic stem cells. Stem Cells *27*, 1836–1846.

Zhao, J.W., Raha-Chowdhury, R., Fawcett, J.W., and Watts, C. (2009). Astrocytes and oligodendrocytes can be generated from NG2+ progenitors after acute brain injury: intracellular localization of oligodendrocyte transcription factor 2 is associated with their fate choice. Eur. J. Neurosci. *29*, 1853–1869.

Zhong, S., Zhang, S., Fan, X., Wu, Q., Yan, L., Dong, J., Zhang, H., Li, L., Sun, L., Pan, N., et al. (2018). A single-cell RNA-seq survey of the developmental landscape of the human prefrontal cortex. Nature *555*, 524–528.

**Stem Cell Reports, Volume *12***

## Supplemental Information

# Pluripotent Stem Cell-Derived Cerebral Organoids Reveal Human Oligodendrogenesis with Dorsal and Ventral Origins

**Hyosung Kim, Ranjie Xu, Ragunathan Padmashri, Anna Dunaevsky, Ying Liu, Cheryl F. Dreyfus, and Peng Jiang**

## Supplemental Experimental Procedures

### Culture and derivation of hPSC cell lines

The OLIG2-GFP knockin hPSCs (hESCs and hiPSCs) were established using a gene-targeting protocol and fully characterized, as reported in our previous studies (Liu et al., 2011; Xue et al., 2016). The OLIG2-GFP hiPSC reporter line was established from the ND2.0 hiPSC line that was obtained from Center for Regenerative Medicine, National Institutes of Health. The hPSCs maintained under a feeder-free condition on a hESC-qualified Matrigel (Corning)-coated dish with mTeSR1 media (STEMCELL Technologies) were used for this study. The hPSCs were passaged approximately once per week by ReLeSR media (STEMCELL Technologies).

### Generation of human forebrain organoids

To avoid non-CNS differentiated tissue and reduce variability in 3D cerebral organoids generation, we used purified pNPCs as the starting population for generating organoids. As shown in Fig. 1A, we induced pNPCs from hPSCs using a small molecule-based protocol (Chen et al., 2016; Li et al., 2011). Briefly, neural differentiation was induced by dual inhibition of SMAD signaling (Chambers et al., 2009) with inhibitors SB431542 (5 μM, Stemgent) and noggin (50 ng/ml, Peprotech) for a week. The embryoid bodies (EB) were then plated on dishes coated with growth factor-reduced Matrigel (BD Biosciences) in the medium consisting of DMEM/F12, 1x N2, and laminin (1 μg/ml; Sigma-Aldrich) for a week. Next, neural rosettes were manually isolated from the expanded area. The isolated neural rosettes were further cultured in pNPC media, composed of a 1:1 mixture of Neurobasal (Thermo Fisher Scientific) and DMEM/F12, supplemented with 1 x N2, 1 x B27-RA (Thermo Fisher Scientific), FGF2 (20 ng/ml, Peprotech), human leukemia inhibitory factor (hLIF, 10 ng/ml, Millipore), CHIR99021 (3 μM, Stemgent), SB431542 (2 μM), and ROCK inhibitor Y-27632 (10 μM, Tocris). To generate organoids, dissociated pNPCs by TrypLE Express (Thermo Fisher Scientific) were placed into low-attachment 96-well plates at a density of 9,000 cells to develop uniform organoids for two days. The pNPC aggregates were then grown and patterned in low-attachment 6-well plates with the treatment of either 5 μM Cyclopamine A (Cyc A; Calbiochem) for dorsalization or dual activation of SHH pathway with sonic hedgehog (SHH; 50 ng/ml, Peprotech) and purmorphamine (Pur; 1 μM, Cayman Chem) for ventralization. Starting from week 5, the DFOs were cultured on an orbital shaker with a speed of 80 rpm/min in neuronal differentiation (ND) medium containing a 1:1 mixture of Neurobasal and DMEM/F12, supplemented with 1 x N2, 1 x B27, BDNF (20 ng/ml, Peptrotech), GDNF (20 ng/ml, Peprotech), dibutyryl-cyclic AMP (1mM, Sigma), and ascorbic acid (200 nM, Sigma). The 5-week-old VFOs were cultured in OPC medium containing DMEM/F12, supplemented with 1 x N2, 1 x B27, FGF2 (10 ng/ml, Peptrotech), PDGF-AA (10 ng/ml, Peprotech). For further neuronal maturation, both DFOs and VFOs were cultured in BrainPhys medium (STEMCELL Technologies). Starting from week 9, organoids were maintained in ND medium supplemented with 3,3,5-Triiodo-L-thyronine sodium salt (T3; 10 ng/ml, Cayman Chem; OL medium) for oligodendroglial differentiation and maturation. FFOs were generated by using a spontaneous fusion method (Bagley et al., 2017; Birey et al., 2017; Xiang et al., 2017) with modifications. Briefly, single week 9 DFO were closely placed with a week 5 VFO by transferring both of them into the round-bottom ultra-low-attachment 96-well plate for 2 days without agitating. Then, the FFOs were transferred to an ultra-low-attachment 6-well plate and cultured for a day without agitating. The next day, the FFOs were maintained with OL medium on an orbital shaker with a speed of 80 rpm/min.

**RNA isolation and qRT-PCR**

Total RNA extracted from organoids with RNAeasy kit (Qiagen) was used to make complementary DNA with a Superscript III First-Strand kit (Invitrogen). The qRT-PCR was performed with TaqMan primers listed in supplementary table 2 on an Abi 7500 Real-Time PCR system. Experimental samples were analyzed by normalization with the expression level of housekeeping gene glyceraldehyde-3-phosphate dehydrogenase (GAPDH). Relative quantification was performed by applying the $2^{-\Delta\Delta Ct}$ method (Livak and Schmittgen, 2001).

**Western blotting**

OLIG2 protein expression and localization in cells were evaluated by immunoblotting using fractionated samples. The nuclear and cytoplasmic fraction was achieved by modification of a reported method (Suzuki et al., 2010). Briefly, organoids were washed with PBS and harvested. Resuspended organoids in 900 ul of ice-cold lysis buffer (0.1% NP40 in PBS) were lysed 10 times through a 25-gauge syringe. Following the second spinning down for 30 seconds, the supernatant was collected as a cytosolic fraction. 3 times washed pellet was lysed in sample buffer containing 1% of SDS. Fractionated proteins were separated on 12% SDS-PAGE gel and transferred onto nitrocellulose membrane. Blots were then blocked in 2% skim milk and incubated with primary antibodies at 4°C overnight. The information for primary antibodies and dilutions is listed in Supplementary table 3. Afterward, the blots were incubated with secondary antibodies conjugated with a fluorophore for an hour at room temperature. Western blot was visualized using Odyssey (LiCor).

**Immunostaining and cell counting**

Organoids fixed with 4% paraformaldehyde were processed and cryo-sectioned for immunofluorescence staining. The information for primary antibodies and dilutions is listed in Table S2. Slides were mounted with the anti-fade Fluoromount-G medium containing 1,40,6-diamidino-2-phenylindole dihydrochloride (DAPI) (Southern Biotechnology). Images were captured with LSM800 confocal microscope. The cells were counted with ImageJ software. At least six fields chosen randomly from three sections of each organoid were counted. For each organoid, at least 400 cells were counted.

**Dye loading and calcium imaging**

For calcium imaging in organoids, DFOs were placed on the growth factor-reduced Matrigel-coated coverslip in 6-well plate for 24 hr. The next day, organoids were loaded with fluo-4 AM (5 μM, Molecular Probes) and 0.04% Pluronic F-127 for 40 minutes and then transferred to the neuronal differentiation (ND) medium for at least 30 minutes before transferring to the submersion-type recording chamber (Warner) superfused at room temperature with artificial CSF (ACSF, mM: 126 NaCl, 3 KCl, 1.25 $NaH_2PO_4$, 1 $MgSO_4$, 2 $CaCl_2$, 26 $NaHCO_3$, and 10 dextrose) saturated with 95% $O_2$/5% $CO_2$. All imaging was performed with a two-photon microscope (Moving Objective Microscope; Sutter Instruments) coupled to a Ti:Sapphire laser (Chameleon Vision II, Coherent). Images were collected with a Nikon water immersion objective (25X, 1.05 NA). Excitation power measured at the back aperture of the objective was typically about 20-30 mW, and laser power was modulated using a Pockels cell. Fluo-4 was excited at 820nm and emission was detected with GaAsP detector

(Hamamatsu Photonics) fitted with a 535/50 bandpass filter and separated by a 565 nm dichroic mirror. ScanImage (v5.1, Vidrio Technologies) software (Pologruto et al., 2003) was used for imaging. Time-lapse imaging was performed every 1 s for 5 minutes and was collected at 512 by 512-pixel resolution. Image analysis was performed using ImageJ software. Regions of interest (ROIs) were placed around soma. Fluorescence was averaged over ROIs placed and expressed as relative fluorescence changes ($\Delta F/F$) after subtraction of background fluorescence from a neighboring region. For each ROI, basal fluorescence was determined during 20 s periods with no $Ca^{2+}$ fluctuation. $Ca^{2+}$ transients were detected when fluorescence intensity reached higher than 2 SD value of baseline fluorescence intensity.

**Electron microscopy**

Organoid samples were fixed with 2% glutaraldehyde, 2% paraformaldehyde, and 0.1M sodium cacodylate in PBS. The selected vibratome sections were post-fixed and processed for electron microscopy (EM) as described in our previous studies (Chen et al., 2016; Jiang et al., 2016). EM images were captured using a high-resolution charge-coupled device (CCD) camera (FEI).

**DNA fingerprinting short tandem repeat (STR) analysis**

STR analysis was performed using GENEprint PowerPlex 16 kit (Promega performed by Cell Line Genetics. LLC). Samples were run in duplicate and blinded to the interpreter to confirm the results. Please note that ND2.0 and OLIG2-GFP hiPSC lines have identical STR genotyping profile, indicating that they are isogenic lines derived from the same parental cell line.

**Supplementary Table 1. STR genotyping profile of ND2.0 hiPSCs and OLIG2-GFP hiPSC reporter line.** STRs of all loci for OLIG2-GFP hiPSCs match to ND2.0 hiPSCs.

| STR Locus | Chr. Location | ND2.0 hiPSCs | | OLIG2-GFP hiPSCs | |
|---|---|---|---|---|---|
| **Amelogenin** | **Xp22.1-22.3 and Y** | **X** | **Y** | **X** | **Y** |
| vWA | 12p12-pter | 17 | 18 | 17 | 18 |
| D8S1179 | 8q | 12 | | 12 | |
| TPOX | 2p23-2pter | 10 | 11 | 10 | 11 |
| FGA | 4q28 | 24 | 26 | 24 | 26 |
| D3S1358 | 3p | 15 | | 15 | |
| THO1 | 11p15.5 | 6 | 9.3 | 6 | 9.3 |
| D21S11 | 21q11-21q21 | 29 | 31.2 | 29 | 31.2 |
| D18S51 | 18q21.3 | 13 | 18 | 13 | 18 |
| Penta E | 15q | 7 | 12 | 7 | 12 |
| D5S818 | 5q23.3-32 | 11 | 12 | 11 | 12 |
| D13S317 | 13q22-q31 | 11 | 12 | 11 | 12 |
| D7S820 | 7q11.21-22 | 12 | | 12 | |
| D16S539 | 15q24-qter | 9 | 11 | 9 | 11 |
| CSF1PO | 5q33.3-34 | 12 | 13 | 12 | 13 |
| Penta D | 21q | 9 | 15 | 9 | 15 |

**Supplementary Table 2. A list of primers used.**

| Gene | Gene expression assay catalog number |
|---|---|
| *ARHGEF9* | HS01003480_m1 |
| *DLX1* | Hs00269993_m1 |
| *EMX1* | Hs00417957_m1 |
| *GAD1* | Hs01065893_m1 |
| *GAPDH* | Hs02758991_g1 |
| *GPHN* | HS00982840_m1 |
| *HIF1A* | Hs00153153_m1 |
| *HOMER1* | Hs01029333_m1 |
| *LEF1* | Hs01547250_m1 |
| *LHX6* | Hs01030941_g1 |
| *MBP* | Hs00921945_m1 |
| *NKX-2-2* | Hs05035641_s1 |
| *OLIG2* | Hs00300164_s1 |
| *PDGFRα* | Hs00998018_m1 |
| *S100β* | Hs00389217_m1 |
| *SHANK3* | Hs01393541_m1 |
| *SLC17A6 (VGLUT2)* | Hs00220439_m1 |
| *SLC17A7 (VGLUT1)* | Hs00220404_m1 |
| *SLC6A1 (GAT1)* | Hs01104475_m1 |
| *TBR2* | Hs00232429_m1 |

**Supplementary Table 3. A list of antibodies used.**

| Antibodies | Vendor/Catalog #. | Type | Dilution |
|---|---|---|---|
| βIIItubulin | Millipore / MAB1637 | Mouse IgG | 1:200 |
| β-tubulin | DSHB / E7 | Mouse IgG | WB (1:1000) |
| c-FOS | Santa Cruz / SC-52 | Rabbit IgG | 1:100 |
| CUX1 | Santa Cruz / SC13024 | Rabbit IgG | 1:500 |
| DCX | Cell Signaling / 4604s | Rabbit IgG | 1:500 |
| EMX1 | Sigma / HPA006421 | Rabbit IgG | 1:1000 |
| FOXG1 | Abcam / ab18259 | Rabbit IgG | 1:500 |
| GFAP | Millipore / AB5804 | Rabbit IgG | 1:1000 |
| GFP | Rockland / 600-141-215 | Goat IgG | 1:1000 |
| GFP | Thermo / MA5-15256 | Mouse IgG | 1:500 |
| GLS | Abcam / ab156876 | Rabbit IgG | 1:250 |
| Ki67 | Cell signaling / 9449 | Mouse IgG | 1:400 |
| Ki67 | Thermo Fisher Scientific / SP6 | Rabbit IgG | 1:200 |
| MAP2 | Millipore / AB3418 | Mouse IgG | 1:500 |
| LHX6 | Abcam / ab22885 | Rabbit IgG | 1:100 |
| MBP | Millipore / MAB386 | Rat IgG | 1:100 |
| NeuN | Millipore / MAB377 | Mouse IgG1 | 1:100 |
| Nestin | Santa Cruz / SC-21249 | Goat IgG | 1:100 |
| NKX2.1(TTF1) | Abcam / ab76013 | Rabbit IgG | 1:200 |
| OLIG2 | Phosphosolutions 1538 | Rabbit IgG | 1:1000; WB (1:2000) |
| PAX6 | GeneTex / GTX11324 | Rabbit IgG | 1:400 |
| PDGFRα | Santa Cruz / SC338 | Rabbit IgG | 1:50 |
| P-Histone H3 | Thermo Fisher Scientific / PA5–17869 | Rabbit IgG | WB(1:1000) |
| PSD95 | Invitrogen 51-6900 | Rabbit IgG | 1:100 |
| S100β | Sigma / S2532 | Mouse IgG | 1:1000 |
| SOX2 | Millipore / AB5603 | Rabbit IgG | 1:100 |
| Synapsin I | Millipore / AB1543P | Rabbit IgG | 1:400 |
| TBR1 | EMD Millipore / AB2261 | Chicken IgG | 1:100 |
| TBR2 | Abcam / AB23345 | Rabbit IgG | 1:100 |
| VGLUT1 | Millipore / AB5905 | Guinea pig IgG | 1:250 |

Antibody dilution for western blotting are specifically marked as WB, and others are for immunostaining.

**References:**


Bagley, J.A., Reumann, D., Bian, S., Levi-Strauss, J., and Knoblich, J.A. (2017). Fused cerebral organoids model interactions between brain regions. Nat Methods *14*, 743-751.

Birey, F., Andersen, J., Makinson, C.D., Islam, S., Wei, W., Huber, N., Fan, H.C., Metzler, K.R.C., Panagiotakos, G., Thom, N.*, et al.* (2017). Assembly of functionally integrated human forebrain spheroids. Nature *545*, 54-59.

Chambers, S.M., Fasano, C.A., Papapetrou, E.P., Tomishima, M., Sadelain, M., and Studer, L. (2009). Highly efficient neural conversion of human ES and iPS cells by dual inhibition of SMAD signaling. Nat Biotechnol *27*, 275-280.

Chen, C., Kim, W.Y., and Jiang, P. (2016). Humanized neuronal chimeric mouse brain generated by neonatally engrafted human iPSC-derived primitive neural progenitor cells. JCI Insight *1*, e88632.

Jiang, P., Chen, C., Liu, X.B., Pleasure, D.E., Liu, Y., and Deng, W. (2016). Human iPSC-Derived Immature Astroglia Promote Oligodendrogenesis by Increasing TIMP-1 Secretion. Cell Rep.

Li, W., Sun, W., Zhang, Y., Wei, W., Ambasudhan, R., Xia, P., Talantova, M., Lin, T., Kim, J., Wang, X.*, et al.* (2011). Rapid induction and long-term self-renewal of primitive neural precursors from human embryonic stem cells by small molecule inhibitors. Proc Natl Acad Sci U S A *108*, 8299-8304.

Liu, Y., Jiang, P., and Deng, W. (2011). OLIG gene targeting in human pluripotent stem cells for motor neuron and oligodendrocyte differentiation. Nat Protoc *6*, 640-655.

Livak, K.J., and Schmittgen, T.D. (2001). Analysis of relative gene expression data using real-time quantitative PCR and the 2(-Delta Delta C(T)) Method. Methods *25*, 402-408.

Pologruto, T.A., Sabatini, B.L., and Svoboda, K. (2003). ScanImage: flexible software for operating laser scanning microscopes. Biomed Eng Online *2*, 13.

Suzuki, K., Bose, P., Leong-Quong, R.Y., Fujita, D.J., and Riabowol, K. (2010). REAP: A two minute cell fractionation method. BMC Res Notes *3*, 294.

Xiang, Y., Tanaka, Y., Patterson, B., Kang, Y.J., Govindaiah, G., Roselaar, N., Cakir, B., Kim, K.Y., Lombroso, A.P., Hwang, S.M.*, et al.* (2017). Fusion of Regionally Specified hPSC-Derived Organoids Models Human Brain Development and Interneuron Migration. Cell Stem Cell *21*, 383-398 e387.

Xue, H., Wu, J., Li, S., Rao, M.S., and Liu, Y. (2016). Genetic Modification in Human Pluripotent Stem Cells by Homologous Recombination and CRISPR/Cas9 System. Methods Mol Biol *1307*, 173-190.